Control-oriented modeling of TCLs

Austin R. Coffman*,‡, Ana Bušić†, and Prabir Barooah*

Abstract-Ensembles of thermostatically controlled loads (TCLs) have the potential to be a valuable resource for the Balancing Authority (BA) of the future. Examples of TCLs include household appliances such as air conditioners, water heaters, and refrigerators. To perform design of a distributed coordination/control algorithm, the BA requires a control oriented model that describes the relevant dynamics of an ensemble. In this work, we develop such a model. We leverage techniques from computational fluid dynamics (CFD) to discretize a pair of Fokker-Planck equations derived in earlier work [1]. The discretized equations are shown to admit a certain factorization that separates the effects of weather and control on the system dynamics. This then infers how one can model a population of TCLs under arbitrary control policies. It also stages the way for computationally efficient control design through convex optimization. Simulation results are provided to elucidate these points.

I. Introduction

An envisioned future for the power grid is one that relies more on renewable generation. However, increased renewable penetration also increases volatility, and will require Balancing Authorities (BA) to utilize varying types of resources to balance the grid. One such example: flexible loads.

Flexible loads are loads that can vary their power consumption, around a nominal value, without affecting the QoS of the load. Nominal refers to the power consumption without control from the BA, and power deviation as the amount deviated from nominal. The nominal consumption, for example, for air conditioners, is largely determined by ambient weather conditions. Examples of flexible loads include, TCLs [2], [3], [4], [5] (e.g., water heaters and air conditioners) pumps for agricultural purposes [6], pool cleaning [3], and heating [7], and HVAC equipment [?]. Since the rated power of some flexible loads is quite small, it is necessary to consider collections of flexible loads. In the following we focus solely on TCLs.

While TCLs are a flexible load, their nominal behavior needs to be altered to take advantage of their flexibility. That is, in order to be utilized as a resource, the BA needs to issue implementable control commands to each TCL that reflects its needs. These inputs modify slightly the nominal behavior of each TCL, so that in aggregate the collection tracks the desired power deviation. Examples of inputs in the current literature include: (i) thermostat set point changes [2], [9], (ii) randomized control algorithms [3], [4], and (iii)

AC and PB are with the Dept. of Mechanical and Aerospace Engineering, University of Florida, Gainesville, FL 32601, USA. AB is with Inria Paris and also with DI ENS, École Normale Supérieure, CNRS, PSL Research University, Paris, France. The research reported here has been partially supported by the NSF through award 1646229 (CPS-ECCS).

direct load control (for example, the priority stack controller within [10]).

From the standpoint of control design, it is also important to have a model that describes the effects of the control input on the ensembles power consumption. Ref. [1] develops a pair of coupled Fokker-Planck equations to model an ensemble of TCLs during nominal operation. The Fokker-Planck equations are partial differential equations (PDEs) that describe the time evolution of a certain probability density function (pdf). Upon discretization, the coupled PDEs turn into coupled ODEs and the pdf turns into a probability mass function (pmf) that holds similar interpretation as the "binned" state common in the literature [5], [11]. However, since the PDEs are developed to model nominal operation it is, in general, a design choice on how to introduce control into this modeling framework.

In this work, we develop a control oriented framework for ensembles of TCLs. This framework is based on discretization of the coupled Fokker-Planck PDEs exposed in [1]. The main contribution is that our discretization allows us to infer a special structure of the resulting discretized system. This structure decomposes the effects of exogenous disturbances, such as weather, and the control input. This structure has the so-called "conditional independence" decomposition appearing as an assumption in the work [12]. There are at least two advantages of the identified structure: (i) it elucidates how one can introduce a control input and (ii) it allows for computationaly efficient control design. To our knowledge, use of discretization to obtain this conditional independence structure is absent from prior literature.

A. Literature review

There are two important ingredients for controlling collections of TCLs: (i) identifying a control input and (ii) modeling the effects of the control input. As previously mentioned, many works modify the modeling framework exposed in [1] to achieve both points (i) and (ii).

Since PDEs are infinite dimensional, some form of a discretization is required for the eventual purpose of control design. After discretization, a finite dimensional population model can be developed. This model is of the form $\nu_{k+1} = \nu_k P_k$ where P_k is a Markov transition matrix and ν_k is a marginal distribution. The works [13], [14], [15] take this route, and ν_k represents the "fraction of flexible loads with state value in a certain bin." Alternative to discretization, one can define this fractional state vector in an ad-hoc fashion and develop population models by analytically computing transition probabilities [11]. It is also possible to estimate the population model through measured data [16] or Monte-Carlo simulation [5].

^{*}University of Florida, †INRIA

[‡]corresponding author, email: bubbaroney@ufl.edu.

To introduce control to the discretized models, one popular approach is to define a vector control input with i^{th} entry as "the fraction of TCLs to switch mode state in bin i" [5], [11], leading to a bilinear control system. Another approach assumes the ability to change the thermostatic set point of each TCL. The effects of this control input can be modeled prior to discretization, and after discretization, like the previous approach, a bilinear control system results [9]. One more approach introduces control by allowing the TCL's mode state to be determined through a randomized control policy [16].

In regards to discretization our approach belongs to the first class of methods, i.e., we discretize the PDEs to obtain a population model of the form $\nu_{k+1} = \nu_k P_k$. However, to introduce control to this control free population model, our approach is different from much of the literature. We study the structure of P_k . Elaborating, the control free population model is based on the TCL's nominal thermostatic policy. Is it then possible to 'factor' this policy out, i.e., rewrite the population model as $\nu_{k+1} = \nu_k \Phi G_k$ so that an arbitrary control policy can be inserted instead? That is, replace the nominal thermostat policy Φ with a control policy that reflects the BA's needs, say $\Phi_k^{\rm BA}$. The answer is affirmative, and this factorization refers to the conditional independence form mentioned prior.

In numerical experiments we evaluate the fidelity of our discretized model by comparing the state of the model to empirical quantities obtained from a simulation of TCLs. In addition, we also offer a preview of control results using the developed model with the identified structure.

The paper proceeds as follows. In Section II the model of the individual TCL is introduced. In Section III the PDEs introduced are discretized and in Section IV the structure of the discretized model is identified. Numerical experiments are reported in Section V and we conclude in Section VI.

II. MODELING: INDIVIDUAL TCL

A. Deterministic Model

An individual TCL has two state variables: (i) a temperature denoted x(t) and (ii) an on/off mode denoted m(t). We consider two models for an individual TCL. The first is the following ODE,

$$\frac{d}{dt}x(t) = f_m(x,t),\tag{1}$$

where

$$f_m(x,t) = -\frac{1}{RC} \left(x - \theta^a(t) \right) - m(t) \frac{\eta P}{C}. \tag{2}$$

The rated electrical power consumption is denoted P with coefficient of performance (COP) η . The parameters R and C denote thermal resistance and capacitance, respectively. The signal $\theta^a(t)$ is the ambient temperature. In the following we identify m(t)=1 and m(t)=0, as well as m(t)=0 and m(t)=0 off. We denote arbitrary temperature values through the variable λ . The thermostat setpoint is denoted as $\lambda^{\rm set}$.

The nominal power for the TCL is the value of P in (2) so that $f_1(\lambda^{\text{set}}, t) = 0$, solving yields:

Nominal Power:
$$\bar{P}^{\text{ind}}(t) = \frac{\theta^a(t) - \lambda^{\text{set}}}{\eta R}$$
. (3)

B. Stochastic Model

The stochastic model is based on the deterministic model. Consider the Itô stochastic differential equation (SDE),

$$dx(t) = f_m(x,t)dt + \sigma^2 dB(t), \tag{4}$$

where B(t) is Brownian motion with parameter $\sigma^2 > 0$, and the quantity $\sigma^2 dB(t)$ captures modeling errors in (1).

a) Nominal thermostat policy: To state the Fokker-Planck PDEs as in [1] we denote the nominal thermostat policy:

$$\lim_{\epsilon \to 0} m(t + \epsilon) = \begin{cases} 1, & x(t) \ge \lambda^{\max}. \\ 0, & x(t) \le \lambda^{\min}. \\ m(t), & \text{o.w.} \end{cases}$$
 (5)

The quantities λ^{\max} and λ^{\min} respectively set the upper and lower temperature limits (i.e., the thermostatic "deadband") for x(t). The nominal policy (5) is only temporary; in Section IV we show how to model the effects of an arbitrary randomized policy.

Now, consider the following marginal pdfs μ_{on} , μ_{off} :

$$\mu_{\text{on}}(\lambda, t)d\lambda = P\left((\lambda < x(t) \le \lambda + d\lambda), \ m(t) = \text{on}\right), \quad (6)$$

$$\mu_{\text{off}}(\lambda, t)d\lambda = P\left((\lambda < x(t) \le \lambda + d\lambda), \ m(t) = \text{off}\right), \quad (7)$$

where $P(\cdot)$ denotes probability, and for now m(t) evolves according to (5). It was shown in [1] that the densities $\mu_{\rm on}$ and $\mu_{\rm off}$ satisfy the Fokker-Planck equations,

$$\frac{\partial}{\partial t}\mu_{\rm on}(\lambda,t) = -\nabla_{\lambda} \left(f_{\rm on}(\lambda,t)\mu_{\rm on}(\lambda,t) \right) + \frac{\sigma^2}{2} \nabla_{\lambda}^2 \mu_{\rm on}(\lambda,t)$$
(8)

$$\frac{\partial}{\partial t}\mu_{\text{off}}(\lambda, t) = -\nabla_{\lambda} \left(f_{\text{off}}(\lambda, t) \mu_{\text{off}}(\lambda, t) \right) + \frac{\sigma^2}{2} \nabla_{\lambda}^2 \mu_{\text{off}}(\lambda, t)$$
(9)

that are coupled through their boundary conditions [1], which are listed later in Section III-A2.

There are at least two ways that the coupled equations (8)-(9) can be used for modeling: (i) to model a *single* TCL and (ii) to model an *ensemble* of TCLs. That is, for (i) the quantities (6)-(7) represent the *probability* that a single TCLs state resides in the respective interval. For (ii) the quantities (6)-(7) represent the *fraction* of TCLs whose state resides in the respective interval. How the equations (8)-(9) (specifically their discretized form) can be used to model an ensemble is discussed further in Section IV-B.

1) Motivation for Stochastic Model: While transport type arguments can be used to develop a pair of coupled advection equations (equations (8)-(9) with $\sigma^2=0$) for the deterministic model [9], the state of these advection equations will not agree with the pointwise in time histogram of a population of TCLs simulated with (1) (see Figure 1). To see

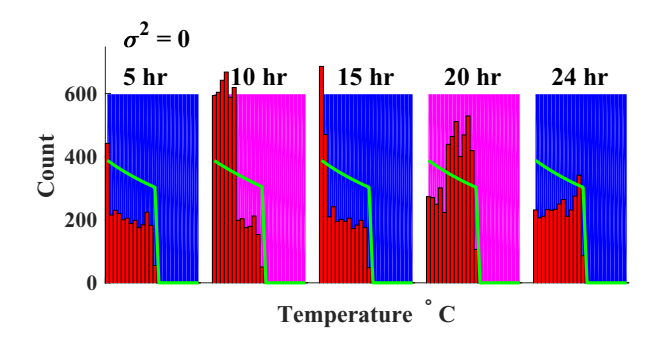


Fig. 1. Discrepancy between the state of the advection equation and the histogram of the population for various time steps. Each histogram is over the temperature state for all of the on TCLs at the specified time.

why, consider the following: without noise TCLs are periodic whereas discretization of the advection equations yields a Markov transition matrix that is irreducible and aperiodic. Hence, the iteration of this transition matrix will converge to a limiting and invariant distribution, whereas the samples from the TCLs will not since the TCL behavior is periodic. This behavior is shown in Figure 1, the discretized state of the advection equation remains relatively constant while the histogram of the ensemble does not; their is no suggestion of convergence even after 24 hours.

Thus, the stochastic model (4) has two advantages: (i) it captures modeling errors and heterogeneity [?] the deterministic model (1) can not, and (ii) it also guarantees a correspondence between simulation samples from (4) and the state of the coupled PDEs (8)-(9) (see Figure 4).

2) Forward thinking motivation: Further, the PDEs that are derived from the stochastic model will be the base of our control oriented model. In the following, we will discretize the PDEs (8)-(9) and then show that the discretized model has special structure. Particularly, the structure elucidates how to model the aggregate under the effects of a arbitrary randomized policy.

III. DISCRETIZATION

In order to be used, the coupled PDEs (8)-(9) need to be spatially and temporally discretized. We will use the finite volume method (FVM) to discretize (8) and (9). In light of the discussion from the previous section, the goal will be to develop a control oriented model. That is, we aim to: (i) obtain a discretized model that agrees well with population quantities (avoids behavior as shown in Figure 1) and (ii) discretize the model in a way that a control input for the BA can be identified. More on point (ii) will be discussed in Section IV, however the discretization here plays a role.

A. Spatial discretization

The layout of the control volumes (CV) is shown in Figure 2. The discretization is achieved by enumerating N, for both the on and off mode state, CV temperature values and their upper and lower boundaries:

$$\begin{split} &\lambda_{\text{on}} = (\lambda_{\text{on}}^i)_{i=1}^N, \ \lambda_{\text{on}}^+ = \lambda_{\text{on}} + \frac{\Delta \lambda}{2}, \ \lambda_{\text{on}}^- = \lambda_{\text{on}} - \frac{\Delta \lambda}{2}, \\ &\lambda_{\text{off}} = (\lambda_{\text{off}}^i)_{i=1}^N, \ \lambda_{\text{off}}^+ = \lambda_{\text{off}} + \frac{\Delta \lambda}{2}, \ \lambda_{\text{off}}^- = \lambda_{\text{off}} - \frac{\Delta \lambda}{2}, \end{split}$$

where $\Delta \lambda$ is the CV width. All intermediate values of λ_{on} and λ_{off} are separated from each other by $\Delta \lambda$. The values in λ_{on}^+ (respectively, λ_{off}^+) are the right edges of the CVs and the values $\lambda_{\rm on}^-$ (respectively, $\lambda_{\rm off}^-$) are the left edges of the CVs, for example, $\lambda_{\rm off}^{1,-}=\lambda^{\rm low}$. The quantities $\lambda^{\rm min}$ and $\lambda^{\rm max}$ specify the thermostat deadband, and are different from the quantities λ^{high} and λ^{low} (see Figure 2).

We denote the i^{th} CV as CV(i) and further adopt the following notational simplifications,

$$\mu_{\text{off}}(\lambda^i, t) \triangleq \mu_{\text{off}}(\lambda^i_{\text{off}}, t), \text{ and } \mu_{\text{on}}(\lambda^i, t) \triangleq \mu_{\text{on}}(\lambda^i_{\text{on}}, t).$$

Highlighted red in Figure 2 are two additional control volumes. These control volumes are added to assist in enforcing boundary conditions that coincide with the thermostat control law (5). Further discussion on this is given in section III-A2.

1) Internal CV's: Consider the RHS of the pde (8) integrated over CV(i):

$$\int_{\text{CV(i)}} \left(\frac{\sigma^2}{2} \frac{\partial^2}{\partial \lambda^2} (\mu_{\text{on}}(\lambda, t)) - \frac{\partial}{\partial \lambda} (f_{\text{on}}(\lambda, t) \mu_{\text{on}}(\lambda, t)) \right) d\lambda$$

$$= \left(\frac{\sigma^2}{2} \frac{\partial}{\partial \lambda} \mu_{\text{on}}(\lambda, t) - f_{\text{on}}(\lambda, t) \mu_{\text{on}}(\lambda, t) \right) \Big|_{\lambda^{i, -}}^{\lambda^{i, +}}, \tag{10}$$

where equality is by the divergence theorem [17]. Note, the points $\lambda^{i,-}$ and $\lambda^{i,+}$ are not control volume variables, but rather the boundaries of a single control volume. Hence, quantities in (10) need to be approximated in terms of the nodal points of the neighboring control volumes. The approximations for the partial derivative are,

$$\frac{\partial}{\partial \lambda} \mu_{\text{on}}(\lambda^{i,+}, t) \approx \frac{\mu_{\text{on}}(\lambda^{i+1}, t) - \mu_{\text{on}}(\lambda^{i}, t)}{\Delta \lambda}, \qquad (11)$$

$$\frac{\partial}{\partial \lambda} \mu_{\text{on}}(\lambda^{i,-}, t) \approx \frac{\mu_{\text{on}}(\lambda^{i}, t) - \mu_{\text{on}}(\lambda^{i-1}, t)}{\Delta \lambda}, \qquad (12)$$

$$\frac{\partial}{\partial \lambda} \mu_{\text{on}}(\lambda^{i,-}, t) \approx \frac{\mu_{\text{on}}(\lambda^{i}, t) - \mu_{\text{on}}(\lambda^{i-1}, t)}{\Delta \lambda}, \tag{12}$$

which correspond to a central difference approximation of the derivative. For the integrated convective term, we use the socalled upwind differencing scheme [17]. This scheme elects the FVM equivalent of a forward or backward difference based on the sign of the convective velocity $f_{on}(\lambda, t)$. When the TCL is on $f_{\rm on}(\lambda,t) < 0$ (i.e., the temperature decreases) the upwind differencing scheme prescribes:

$$f_{\text{on}}(\lambda^{i,-}, t)\mu_{\text{on}}(\lambda^{i,-}, t) = f_{\text{on}}(\lambda^{i,-}, t)\mu_{\text{on}}(\lambda^{i}, t), \text{ and } (13)$$

$$f_{\text{on}}(\lambda^{i,+}, t)\mu_{\text{on}}(\lambda^{i,+}, t) = f_{\text{on}}(\lambda^{i,+}, t)\mu_{\text{on}}(\lambda^{i+1}, t).$$
 (14)

When the TCL is off $f_{on}(\lambda, t) > 0$ (i.e., the temperature increases) the upwind differencing scheme prescribes:

$$f_{\text{off}}(\lambda^{i,-},t)\mu_{\text{off}}(\lambda^{i,-},t) = f_{\text{off}}(\lambda^{i,-},t)\mu_{\text{off}}(\lambda^{i-1},t), \quad (15)$$

$$f_{\text{off}}(\lambda^{i,+}, t)\mu_{\text{off}}(\lambda^{i,+}, t) = f_{\text{off}}(\lambda^{i,+}, t)\mu_{\text{off}}(\lambda^{i}, t). \tag{16}$$

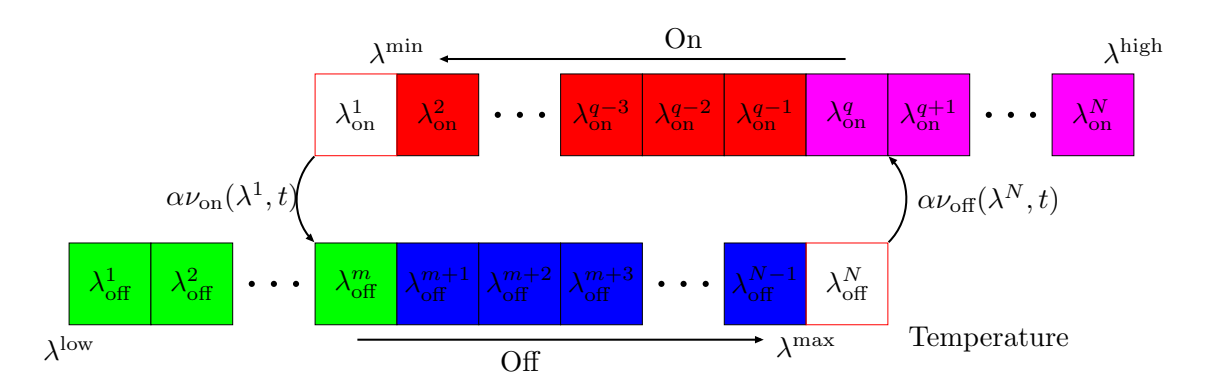


Fig. 2. The control volumes (CVs). The colors correspond to the colors found in Figure 3. The values in each CV represent the nodal temperature for the CV. The arrows describe the sign of the convection of the TCL through the CVs.

Now returning to the discretization of the PDE (8) over an arbitrary internal CV. We approximate the LHS of (8) integrated over the control volume as,

$$\int_{\text{CV(i)}} \frac{\partial}{\partial t} \mu_{\text{on}}(\lambda, t) d\lambda \approx \frac{d}{dt} \mu_{\text{on}}(\lambda^{i}, t) \Delta\lambda = \frac{d}{dt} \nu_{\text{on}}(\lambda^{i}, t),$$

where $\nu_{\text{on}}(\lambda^i, t) \triangleq \mu_{\text{on}}(\lambda^i, t) \Delta \lambda$. We have used the ordinary differential as it will be the only differential to appear in the following. Now, denote the following

$$D \triangleq \frac{\sigma^2}{(\Delta \lambda)^2}$$
, and $F_{\text{on}}^i(t) \triangleq \frac{f_{\text{on}}(\lambda^i, t)}{\Delta \lambda}$, (17)

where the quantities $F_{\rm off}^i(t)$, $F_{\rm on}^{i,+}(t)/F_{\rm off}^{i,+}(t)$, and $F_{\rm on}^{i,-}(t)/F_{\rm off}^{i,-}(t)$ are defined analogously. Now inserting the central difference approximation and upwind difference approximation in (10) and combining it with the approximation of the LHS of (8) we have,

$$\frac{d}{dt}\nu_{\text{on}}(\lambda^{i},t) = \left(F_{\text{on}}^{i,-}(t) - D\right)\nu_{\text{on}}(\lambda^{i},t) + \frac{D}{2}\nu_{\text{on}}(\lambda^{i-1},t) + \left(\frac{D}{2} - F_{\text{on}}^{i,+}(t)\right)\nu_{\text{on}}(\lambda^{i+1},t). \tag{18}$$

The spatial discretization for the pde (9) is similar and yields,

$$\frac{d}{dt}\nu_{\text{off}}(\lambda^{i}, t) = \frac{D}{2}\nu_{\text{off}}(\lambda^{i+1}, t) - \left(F_{\text{off}}^{i,+}(t) + D\right)\nu_{\text{off}}(\lambda^{i}, t) + \left(\frac{D}{2} + F_{\text{off}}^{i,-}(t)\right)\nu_{\text{off}}(\lambda^{i-1}, t). \tag{19}$$

2) Boundary CV's: The boundary CVs are the CVs associated with the nodal values: $\lambda_{\rm on}^1$, $\lambda_{\rm on}^q$, $\lambda_{\rm on}^N$, $\lambda_{\rm off}^1$, $\lambda_{\rm off}^m$, and $\lambda_{\rm off}^N$. The superscript, for example the integer q in $\lambda_{\rm on}^q$ represents the CV index. All boundary CVs can be seen in Figure 2. Discretization of the boundary CVs requires care for atleast two reasons. First, this is typically where one introduces the BCs of the PDE into the numerical approximation. Secondly, on finite domains the endpoints present challenges, for example, there is no variable $\mu_{\rm on}(\lambda^{N+1},t)$ for computation of the derivative values for node $\lambda_{\rm on}^N$.

The BC's for the coupled PDEs (8)-(9) are [1]:

Absorbing Boundaries:

$$\mu_{\text{on}}(\lambda^{\min}, t) = \mu_{\text{off}}(\lambda^{\max}, t) = 0.$$
 (20)

Conditions at Infinity:

$$\mu_{\text{on}}(+\infty, t) = \mu_{\text{off}}(-\infty, t) = 0.$$
 (21)

Conservation of Probability:

$$\frac{\partial}{\partial \lambda} \left[\mu_{\text{on}}(\lambda^{q,-}, t) - \mu_{\text{on}}(\lambda^{q-1,+}, t) - \mu_{\text{off}}(\lambda^{N-1,+}, t) \right] = 0.$$
(22)

$$\frac{\partial}{\partial \lambda} \left[\mu_{\text{off}}(\lambda^{m,+}, t) - \mu_{\text{on}}(\lambda^{2,-}, t) - \mu_{\text{off}}(\lambda^{m+1,-}, t) \right] = 0.$$
(23)

Continuity:

$$\mu_{\text{on}}(\lambda^{q,-}, t) = \mu_{\text{on}}(\lambda^{q-1,+}, t).$$
 (24)

$$\mu_{\text{off}}(\lambda^{m,+}, t) = \mu_{\text{off}}(\lambda^{m+1,-}, t).$$
 (25)

As we will see, implementation of some of the above conditions will require a bit of care. However, some are quite trivial to enforce. For example, by default, the continuity conditions (24) and (25) are satisfied due to our choice of CV structure, since, for example, for any i we have $\lambda_{\rm off}^{i,-} = \lambda_{\rm off}^{i-1,+}$ and $\lambda_{\rm off}^{i,+} = \lambda_{\rm off}^{i+1,-}$.

Now focusing on the conditions at infinity BC (21), we enforce instead the following conditions:

$$\frac{\partial}{\partial \lambda} \mu_{\rm off}(\lambda^{1,-},t) = 0$$
, and $\frac{\partial}{\partial \lambda} \mu_{\rm on}(\lambda^{N,+},t) = 0$. (26)

The reason for this is because our computational domain cannot extend to infinity, where the BC (21) is required to hold. Practically, the temperature values $\lambda_{\rm off}^1$ and $\lambda_{\rm on}^N$ are quite far away from the deadband and so the density here will be near zero anyways.

Now, consider the spatial discretization of the CVs associated with the BC at infinity. First considering the CV associated with the temperature λ_{off}^1 , we have that the differential

equation is

$$\frac{d}{dt}\nu_{\text{off}}(\lambda^{1},t) = \left(-F_{\text{off}}^{1,+}(t) - \frac{D}{2}\right)\nu_{\text{off}}(\lambda^{1},t) + \left(\frac{D}{2} + F_{\text{off}}^{2,-}(t)\right)\nu_{\text{off}}(\lambda^{2},t). \tag{27}$$

Considering the CV associated with the temperature λ_{on}^{N} , we have

$$\frac{d}{dt}\nu_{\text{on}}(\lambda^{N}, t) = \left(F_{\text{on}}^{N,+}(t) - \frac{D}{2}\right)\nu_{\text{on}}(\lambda^{N}, t) + \left(\frac{D}{2} - F_{\text{on}}^{N,+}(t)\right)\nu_{\text{on}}(\lambda^{N-1}, t).$$
(28)

In the above we make the assumption that $\nu_{\rm off}(\lambda^{1,-}-\Delta\lambda,t)=0$ and $\nu_{\rm on}(\lambda^{N,+}+\Delta\lambda,t)=0$.

Now focus on the absorbing boundary (20) and conservation of probability (22)-(23) boundary conditions. These BCs have the following meaning. The condition (20) clamps the density at the end of the deadband to zero. BC (22) reads: the net-flux across the temperature value $\lambda_{\rm on}^q$ is equal to the flux of density going from off to on. In order to enforce both (22) and (23) we will model the flux due to TCLs switching as sources/sinks. Before doing this, we mention some conceptual issues with enforcing the BC (20).

Problematically, a TCL's state trajectory will never satisfy the BC (20) since to switch its mode state the TCLs temperature sensor will have to register a value outside the deadband. That is, it is possible to enforce the BC (20), however the developed model would have a discrepancy with the behavior of a TCL. To combat this, we introduce two additional CV's associated with the temperatures $\lambda_{\rm on}^1$ and $\lambda_{\rm off}^N$, which are the ones outlined in red in Figure 2. We then transfer the BC (20) to one on the added CVs, where the transferred BC is now

$$\mu_{\text{on}}(\lambda^{1,-},t) = \mu_{\text{off}}(\lambda^{N,+},t) = 0.$$
 (29)

As mentioned, to enforce the conservation of probability BC we use a source/sink type argument, which we also enforce on the added CVs. To see what we mean by source/sink argument, consider the following: some rate of TCLs are transferred out of the CV $\lambda_{\rm off}^N$ and into the CV $\lambda_{\rm on}^q$ (as depicted in Figure 2) due to thermostatic control. Since during operation, any TCL within the CV $\lambda_{\rm off}^N$ would immediately switch on, we model the sink as simply $-\nu_{\rm off}(\lambda^N,t)$. The rate of the sink is then given as $-\gamma\nu_{\rm off}(\lambda^N,t)$, where $\gamma>0$ is a modeling choice and a constant of appropriate units that describes the discharge rate. We shortly given insight on how to elect a value for γ . Now discretizing the CV corresponding to the nodal value $\lambda_{\rm off}^N$ subject to the BC (29) and the sink $-\nu_{\rm off}(\lambda^N,t)$ we obtain,

$$\frac{d}{dt}\nu_{\rm off}(\lambda^N,t) = \left(\frac{D}{2} + F_{\rm off}^{N,-}(t)\right)\nu_{\rm off}(\lambda^{N-1},t) - \alpha\nu_{\rm off}(\lambda^N,t),$$
The matrix $\mathcal{A}(t)$ contains all of the coefficients from the individual ode's developed so far from spatial discretization. In

where $\alpha=(\gamma+D)$. In obtaining the above, we have made the reasonable assumption that $\nu_{\rm off}(\lambda^{N,+}+\Delta\lambda,t)=0$. The quantity $\alpha\nu_{\rm off}(\lambda^N,t)$ represents the rate of change of density from the CV $\lambda^N_{\rm off}$ to the CV $\lambda^q_{\rm on}$, as depicted in

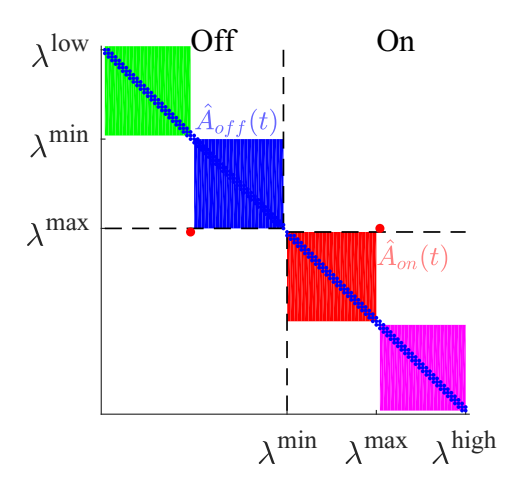


Fig. 3. Sparsity pattern of the matrix A(t) for N=51 CVs for both the on and off state. The colors correspond to the colors found in Figure 2.

Figure 2. Consequently, to conserve probability, we must add this quantity as a source to the ode for the CV λ_{on}^q , i.e.,

$$\frac{d}{dt}\nu_{\rm on}(\lambda^q, t) = \dots + \alpha\nu_{\rm off}(\lambda^N, t). \tag{31}$$

The dots in equation (31) represent the portion of the dynamics for the standard internal CV (i.e., the RHS of (18)) for the temperature node $\lambda_{\rm on}^q$. A similar argument is used for the BC (23) with the CV's $\lambda_{\rm on}^1$ and $\lambda_{\rm off}^m$, and the corresponding differential equations are,

$$\frac{d}{dt}\nu_{\text{on}}(\lambda^1, t) = \left(\frac{D}{2} - F_{\text{on}}^{1,+}(t)\right)\nu_{\text{on}}(\lambda^2, t) - \alpha\nu_{\text{on}}(\lambda^1, t),\tag{32}$$

$$\frac{d}{dt}\nu_{\text{off}}(\lambda^m, t) = \dots + \alpha\nu_{\text{on}}(\lambda^1, t). \tag{33}$$

Practically, once the differential equations are discretized in time with timestep Δt one will then elect γ so that $\alpha = (\Delta t)^{-1}$. With this choice, the discretized equations have the interpretations that all mass starting in state $\nu_{\rm off}(\lambda^N,\cdot)$ at time t is transferred out by time $t+\Delta t$ into the state $\nu_{\rm on}(\lambda^q,\cdot)$.

3) Overall system: Denoting the state of the overall system at time t as the row vector, $\nu(t) = [\nu_{\text{off}}(t), \nu_{\text{on}}(t)]$ with

$$\nu_{\text{off}}(t) = [\nu_{\text{off}}(\lambda^1, t), \dots, \nu_{\text{off}}(\lambda^N, t)], \tag{34}$$

$$\nu_{\text{on}}(t) = [\nu_{\text{on}}(\lambda^1, t), \dots, \nu_{\text{on}}(\lambda^N, t)], \tag{35}$$

and combing the odes: (18) and (19) for all of the internal CVs and (27), (28), (30), (31), (32), (33) for the BC CVs. We obtain the linear time varying system,

$$\frac{d}{dt}\nu^{T}(t) = \mathcal{A}(t)\nu^{T}(t). \tag{36}$$

The matrix $\mathcal{A}(t)$ contains all of the coefficients from the individual ode's developed so far from spatial discretization. In the following, it will be convenient to view the dynamics (36) in their transposed form

$$\frac{d}{dt}\nu(t) = \nu(t)A(t),\tag{37}$$

with $A(t) = \mathcal{A}^T(t)$. We have included the sparsity pattern of A(t) in Figure 3. The matrix A(t) also satisfies the properties of a transition rate matrix, described in the following lemma.

Lemma 1. For all t, the matrix A(t) is a transition rate matrix, that is, it satisfies for all t,

(*i*):
$$A(t)\mathbb{1} = 0$$
.

(ii):
$$\forall i, A_{i,i}(t) \leq 0$$
, and $\forall j \neq i A_{i,j}(t) \geq 0$.

Proof. The FVM method is well known to conserve mass, so that property (i) is readily satisfied. Property (ii) can be inferred from the each individual CV equation.

B. Temporal discretization

To temporally integrate the dynamics (37) we use a first order Euler approximation with time step $\Delta t > 0$. Making the identifications $\nu_{k+1} \triangleq \nu(t_{k+1})$, $\nu_k \triangleq \nu(t_k)$, and $A_k \triangleq A(t_k)$ we have

$$\nu_{k+1} = \nu_k P_k, \text{ with } P_k = I + \Delta t A_k. \tag{38}$$

In the continuous time setting elements of the vector $\nu(t)$ were referred to as, for example, $\nu_{\rm on}(\lambda^i,t)$. The counterpart to this, in the discrete time setting, is referring to elements of ν_k as, for example, $\nu_{\rm on}[\lambda^i,k]$.

IV. IDENTIFYING STRUCTURE AND THE CONTROL INPUT

We started with the PDEs (8)-(9), and in the previous section completely discretized them. Recall, that in the original work [1] the PDEs were developed under the assumption that the mode state m(t) evolved according to (5). Hence, from the viewpoint of control, we still need to identify the control input since the final discretized model (38) has no control input. The goal of this section is to identify any structure that may be present in the matrix P_k appearing in (38) and to then exploit it for purposes of introducing a control input. Key to doing this is the result that P_k is a transition matrix.

Lemma 2. Denote the i^{th} diagonal element of the matrix A_k as $[A_k]_{i,i}$. The matrix P_k is a transition matrix if,

$$\forall i, \text{ and } \forall k, \quad 0 < \Delta t \leq |[A_k]_{i,i}|^{-1}.$$

Proof. From Lemma 1 we have that $P_k \mathbb{1} = I \mathbb{1} + \Delta t A_k \mathbb{1} = \mathbb{1}$ since $A_k \mathbb{1} = 0$. Also from Lemma 1, every element of A_k is non-negative, save for the diagonal elements. Under the hypothesis on A_k , then every diagonal element of $I + \Delta t A_k$ will be in [0,1].

Now, when the conditions of Lemma 2 are met P_k is a transition matrix and hence each ν_k can be viewed as a marginal distribution if $\nu_0\mathbb{1}=1$ and $\nu[\cdot,0]>0$. The structure of this marginal is given from (6) for the on state (a similar interpretation holds for the off state) as,

$$\nu_{\text{on}}[\lambda^i, k] = \mathsf{P}\left(x(t_k) \in \mathsf{CV}(i), \ m(t_k) = \mathsf{on}\right),\tag{39}$$

where $x(t_k)$ is the temperature. Now denote, $x_k \triangleq x(t_k)$, $m_k \triangleq m(t_k)$, and

$$I_k \triangleq \sum_{i=1}^{N} i \mathbf{I} \Big(x_k \in \mathrm{CV}(i) \Big),$$
 (40)

where $\mathbf{I}(\cdot)$ is the indicator function. The quantity I_k indicates which CV the TCLs temperature resides in at time k. Using I_k we rewrite $\nu_{\text{on}}[\lambda^i, k]$ and $\nu_{\text{off}}[\lambda^i, k]$ as,

$$\nu_{\text{on}}[\lambda^{i}, k] = P(I_{k} = i, m_{k} = \text{on}), \text{ and}$$
 (41)

$$\nu_{\text{off}}[\lambda^i, k] = P(I_k = i, \ m_k = \text{off}). \tag{42}$$

A. Conditional independence of P_k

From (41) and (42), the matrix P_k (with the conditions of Lemma 2 satisfied) is the transition matrix for the joint process (I_k, m_k) . In the following, we refer to the values of I_k with i and j and the values of m_k with u and v. We introduce the following notation to refer to the elements of the transition matrix P_k : $P_w((i, u), (j, v)) \triangleq$

$$P(I_{k+1} = j, m_{k+1} = v \mid I_k = i, m_k = u, \theta_k^a = w).$$

Recall, the matrix P_k is derived for the nominal thermostat policy. We will now show that the matrix P_k can be written as the product of two matrices. One depending on the nominal thermostat policy and one depending on weather and TCL system dynamics. That is, to show that each element of the matrix P_k can be written as,

$$P_w((i, u), (j, v)) = \phi_u(v \mid j)G_w((i, u), j)$$
(43)

where: $G_w((i, u), j) \triangleq$

$$P(I_{k+1} = j \mid I_k = i, m_k = u, \theta_k^a = w), \text{ and}$$
 (44)

$$\phi_u(v \mid j) \triangleq P(m_{k+1} = v \mid I_{k+1} = j, m_k = u).$$
 (45)

The quantity $\phi_u(v \mid j)$ is the factor that depends on the nominal thermostat policy. As such, in the following we describe $\phi_u(v \mid j)$ as a policy. The vectorized form of the policies are,

$$\phi_{\text{off}} \triangleq \phi_{\text{off}}(\text{on } | \cdot), \quad \text{and} \quad \phi_{\text{on}} \triangleq \phi_{\text{on}}(\text{off } | \cdot), \quad (46)$$

where ϕ_{off} , $\phi_{\text{on}} \in \mathbb{R}^N$. The factorization (43) is represented in matrix form as,

$$P_k = \Phi G_k, \tag{47}$$

where $\Phi \in \mathbb{R}^{2N \times 4N}$ and $G_k \in \mathbb{R}^{4N \times 2N}$. The subscript k on G_k is to denote its dependence on the continuous time varying ambient temperature θ_k^a . The factorization (47) is paramount as it tells us how the nominal thermostat policy and weather independently contribute to the overall dynamics. Inversely, it then informs us how to define the matrix P_k for a different policy that can act as a control input for the BA.

We show the factorization (47) through construction, i.e., we find a matrix Φ and G_k that simultaneously satisfy (47) and (43). We start this construction through the sparsity structure shown for A(t) in Figure 3. Based on shaded

regions of the matrix A(t) shown in Figure 3, we define the following:

$$P_k^{\text{on}} = I + \Delta t A_k^{\text{on}}$$
, and $P_k^{\text{off}} = I + \Delta t A_k^{\text{off}}$, (48)

$$\hat{P}_k^{\mathrm{on}} = I + \Delta t \hat{A}_k^{\mathrm{on}}, \text{ and } \hat{P}_k^{\mathrm{off}} = I + \Delta t \hat{A}_k^{\mathrm{off}}.$$
 (49)

More precisely A_k^{on} (respectively, A_k^{off}) is the matrix containing the coefficients of the spatially discretized PDE (8) (respectively, PDE (9)) evaluated at time t_k . That is, A_k^{on} is the matrix that corresponds to the bottom-right quadrant encompassed by the dashed black line in Figure 3. The matrix \hat{A}_k^{on} (respectively, \hat{A}_k^{off}) holds the same interpretation as A_k^{on} (respectively, A_k^{off}) except restricted to the control volumes between $[\lambda^{\min}, \lambda^{\max}]$. We additionally define the following matrices,

$$S_k^{\text{on}} = \begin{bmatrix} \mathbf{0} & \mathbf{0} \\ \hat{P}_k^{\text{on}} & \mathbf{0} \end{bmatrix}, \text{ and } S_k^{\text{off}} = \begin{bmatrix} \mathbf{0} & \hat{P}_k^{\text{off}} \\ \mathbf{0} & \mathbf{0} \end{bmatrix}$$
 (50)

which will be used to show the factorization (43) in the following lemma.

Lemma 3. Let e^{ℓ} be the ℓ^{th} canonical basis vector in \mathbb{R}^N . Let $\phi_{off} = e^1$ and $\phi_{on} = e^N$ then denote $\Phi_{on} = diag(\phi_{on})$ and $\Phi_{off} = diag(\phi_{off})$. Now, let Φ and G_k be given as,

$$\Phi = \begin{bmatrix} I - \Phi_{off} & \Phi_{off} & 0 & 0\\ 0 & 0 & \Phi_{on} & I - \Phi_{on} \end{bmatrix}$$
 (51)

$$G_{k} = \begin{bmatrix} 0 & S_{k}^{on} & 0 & P_{k}^{off} \\ P_{k}^{on} & 0 & S_{k}^{off} & 0 \end{bmatrix}^{T}.$$
 (52)

If $\alpha = (\Delta t)^{-1}$ (appearing in (31) and (33)), then $P_k = \Phi G_k$.

Proof. If $\alpha = (\Delta t)^{-1}$, the diagonal elements of A_k with α in them will go to zero and the non diagonal elements will go to 1. These non-diagonal elements with value 1 are the red dots in Figure 3 and encapsulate the thermostat control law. Thus the construction of Φ with the canonical basis vectors. Now, multiplying out the matrix we have

$$\Phi G_k = \begin{bmatrix} (I - \Phi_{\text{off}}) P_k^{\text{on}} & \Phi_{\text{off}} S_k^{\text{on}} \\ \Phi_{\text{on}} S_k^{\text{on}} & (I - \Phi_{\text{on}}) P_k^{\text{on}} \end{bmatrix}$$
(53)

where $(I - \Phi_{\text{off}})P_k^{\text{on}}$ (respectively, $(I - \Phi_{\text{on}})P_k^{\text{off}}$) is the matrix P_k^{on} (respectively, P_k^{off}) but with the last (respectively, first) row zeroed out. The exact opposite statement is true for $\Phi_{\rm off} P_k^{\rm on}$ and $\Phi_{\rm on} P_k^{\rm off}$. Hence, by definition of the matrices in G_k we have $P_k = \Phi G_k$ where each non-zero element holds the interpretation (43).

The conditional independence factorization has been a useful assumption in the design of algorithms in [12]. In the present it is a byproduct of our spatial and temporal discretization of the PDEs (8)-(9). There are at least two important consequences of the factorization result from Lemma 3. The first one is described in the following corollary.

Corollary 1. For the nominal thermostat policy (5), our spatial and temporal discretization scheme induces the degenerate (deterministic) stationary policy:

$$P(m_k = on \mid I_k = N, m_{k-1} = off) = 1,$$

 $P(m_k = off \mid I_k = 1, m_{k-1} = on) = 1,$

and zero otherwise.

Proof. Identifying the non zero elements of the policies ϕ_{on} and $\phi_{\rm off}$ in Lemma 3 with the respective state values gives the desired result.

Hence, the policy induced by the nominal thermostat policy (5) and described in Corollary 1 is exactly the nominal thermostat policy. This recovery of the original control law gives confidence in the underlying spatial and temporal discretization schemes. The second important consequence of Lemma 3 is that it informs us how to define the dynamics of the marginals (41) under a different policy than the nominal thermostat policy.

B. Introducing control + aggregate model

In light of Lemma 3, we can now introduce an arbitrary randomized policy in place of the degenerate nominal thermostat policies described in Corollary 1. From the viewpoint of the BA this randomized policy is the control input that it must design so the TCLs meet it's needs. To distinguish from ϕ_{off} and ϕ_{on} in the prior section we denote the newly introduced policies with the superscript 'BA' and describe them as 'BA control policies.' For example, electing policies $\phi_{\rm on}^{\rm BA}$ and $\phi_{\rm off}^{\rm BA}$ as,

$$\phi_{\text{off}}^{\text{BA}}(\text{on } | j) = \begin{cases}
\kappa_{j}^{\text{on}}, & (m+1) \leq j \leq (N-1). \\
1, & j = N. \\
0, & \text{o.w.}
\end{cases}$$

$$\phi_{\text{on}}^{\text{BA}}(\text{off } | j) = \begin{cases}
\kappa_{j}^{\text{off}}, & 2 \leq j \leq (q-1). \\
1, & j = 1. \\
0, & \text{o.w.}
\end{cases}$$
(54)

$$\phi_{\text{on}}^{\text{BA}}(\text{off} \mid j) = \begin{cases} \kappa_{j}^{\text{off}}, & 2 \le j \le (q-1).\\ 1, & j = 1.\\ 0, & \text{o.w.} \end{cases}$$
 (55)

with $\phi_{\mathrm{off}}^{\mathrm{BA}}(\mathrm{off}\mid\cdot)=1-\phi_{\mathrm{off}}^{\mathrm{BA}}(\mathrm{on}\mid\cdot)$ and $\phi_{\mathrm{on}}^{\mathrm{BA}}(\mathrm{on}\mid\cdot)=1-\phi_{\mathrm{on}}^{\mathrm{BA}}(\mathrm{off}\mid\cdot)$ and $\kappa_{j}^{\mathrm{on}},\kappa_{j}^{\mathrm{off}}\in[0,1]$ for all j will preserve the factorization interpretation found in Lemma 3. The policies could also be time varying, for example: $\kappa_j^{\text{off}}[k]$ and $\kappa_j^{\text{on}}[k]$. The dependence of the policies on time is denoted as $\phi_{\rm off}^{\rm BA}[k]$ and $\phi_{\text{on}}^{\text{BA}}[k]$.

We have required $\phi_{\text{off}}^{\text{BA}}(\text{on } \mid j) = 0 \text{ for } 1 \leq j \leq m \text{ since}$ the temperatures corresponding to these indices are below the permitted deadband temperature, λ^{\min} . Hence, turning on at these temperature does not make physical sense. The arguments for the zero elements in $\phi_{\rm on}^{\rm BA}$ are symmetric.

Remark 1. From the individual TCLs perspective, implementation of BA control policies of the form (54)-(55) is straightforward: (i) the TCL measures its current state, (ii) the TCL "bins" this state value according to (40) and (iii) the TCL flips a coin to decide its next on/off state according to the probabilities given in (54)-(55). Note that the randomized policies are wrapped inside of the nominal thermostat policy (5), so that both the BA control policy and nominal thermostat policies are equivalent in enforcing the temperature constraint.

In the following, we denote Φ_k^{BA} as the matrix with structure (51) but containing any time varying BA control policies $\phi_{\text{off}}^{\text{BA}}[k]$ and $\phi_{\text{on}}^{\text{BA}}[k]$ that satisfy the requirements specified in (54) and (55), respectively. With this, the *control oriented aggregate model* is the following discrete time system

$$\nu_{k+1} = \nu_k \Phi_k^{\text{BA}} G_k, \quad \gamma_k = \nu_k C_{\text{on}}, \tag{56}$$

where $C_{\text{on}} = [\mathbf{0}^T, P_{\text{agg}} \mathbb{1}^T]^T$ with $P_{\text{agg}} \triangleq P \mathsf{N}_{\text{tcl}}$. The control input for this model is Φ_k^{BA} , which translates to an input locally for each TCL (see previously Remark 1). The nominal consumption for the ensemble expressed in terms of the nominal consumption of the individual TCL (3) is,

$$\bar{P}_k \triangleq \mathsf{N}_{\mathsf{tcl}} \bar{P}_k^{\mathsf{ind}}.$$
 (57)

The nominal consumption is time varying due to its dependence on the time varying ambient temperature (see (3)). This quantity, modulo a constant, represents the fraction of TCLs that are on in nominal operation.

V. NUMERICAL EXAMPLES

We now conduct numerical experiments to show: (i) how the PDEs (8)-(9) can be used to model an ensemble of TCLs and (ii) how the framework can be used to design BA control policies so that the ensemble of TCLs track a power reference signal. Each TCL is indexed by ℓ and the total number of TCLs is denoted N_{tcl}. For example, m_k^ℓ and I_k^ℓ are the mode and binned temperature of the ℓ^{th} TCL at time k.

A. Evaluating the aggregate model

Two empirical ensemble quantities of interest are:

$$Y_k \triangleq P \sum_{\ell=1}^{\mathsf{N}_{\mathsf{tcl}}} m_k^\ell, \text{ and } H_k[i,u] \triangleq \sum_{\ell=1}^{\mathsf{N}_{\mathsf{tcl}}} \mathbf{I} \big(I_k^\ell = i, m_k^\ell = u \big),$$

which are the total power consumption and histogram of the ensemble, respectively. They are empirical counterparts to the state (histogram) and output of the aggregate model (56).

We now compare the empirical and analytical aggregate quantities in simulation. The results are shown in Figure 4 and 5 for $N_{tcl} = 50000$. The mode state of each TCL evolves according to a BA control policy that satisfies the structural requirements in (54) and (55) and is relatively similar to the nominal thermostat policy (Corollary 1). The temperature evolution evolves according to a simulated version of (4). We see the state ν_k matches well the histogram H_k of the ensemble (Figure 4) and the output γ_k matches well the ensembles power consumption Y_k (Figure 5).

B. Controlling the Ensemble

Due to space limitations, a full description of the control algorithm is not possible. However, as a preview we present simulation results from the algorithm in Figure 6. The reference signal r_k shown in Figure 6 is an arbitrarily generated sum of sinusoids added to the nominal power, \bar{P}_k . The ambient air temperature used to compute \bar{P}_k is time varying and is obtained from weatherunderground.com for a typical summer day in Gainesville, Fl.

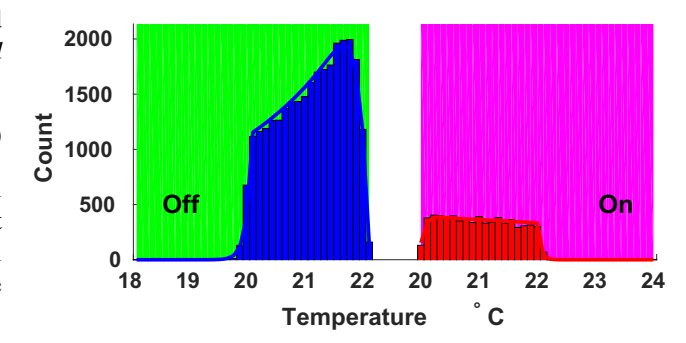


Fig. 4. Histogram of the ensemble H_k compared with the marginals $\nu_{\mbox{off}}[k]$ and $\nu_{\mbox{on}}[k]$ obtained from the aggregate model.

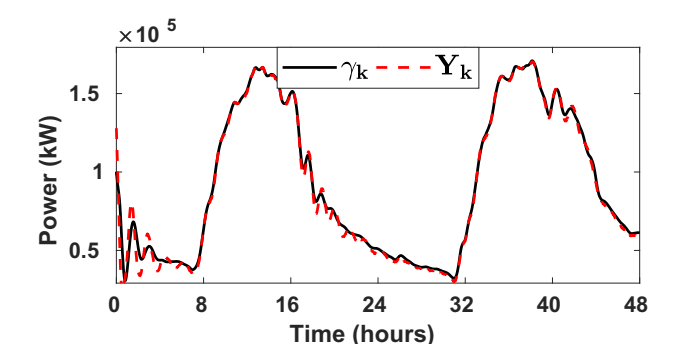


Fig. 5. The total power consumption Y_k compared with the output of the aggregate model, γ_k .

The control algorithm amounts to solving a convex optimization problem, and its facilitation is in large part due to the identified structure. Essentially, the optimization problem utilizes the model (56) to obtain a string of optimal randomized BA control policies $\Phi_k^{\text{BA},*}$. The BA can then send these policies to each TCL, where implementation is as described in 1. Each TCL using the designed BA control policies has the effect of the ensemble tracking r_k , as shown in Figure 6.

VI. CONCLUSION

We discretize the Fokker-Planck equations, derived in the past literature [1], for a population of TCLs. The discretized

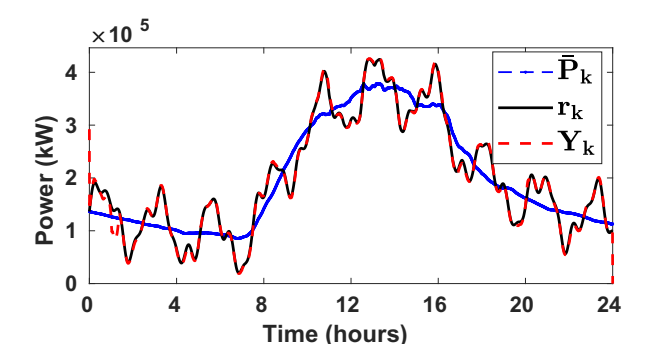


Fig. 6. The power consumption of the ensemble Y_k compared with the desired reference r_k and the baseline power \bar{P}_k .

equations are then shown to satisfy a certain factorization: the effects of weather and control factor out. The discretized model is verified in simulation, and preliminary results of using the model with its identified factorization for control are shown. Future work entails incorporating the cycling state into the obtained model.

REFERENCES

- R. Malhame and C.-Y. Chong, "Electric load model synthesis by diffusion approximation of a high-order hybrid-state stochastic system," *IEEE Transactions on Automatic Control*, vol. 30, no. 9, pp. 854–860, 1985
- [2] D. Callaway and I. Hiskens, "Achieving controllability of electric loads," *Proceedings of the IEEE*, vol. 99, no. 1, pp. 184–199, 2011.
- [3] Y. Chen, M. U. Hashmi, J. Mathias, A. Bušić, and S. Meyn, "Distributed control design for balancing the grid using flexible loads," in *IMA Volume on the Control of Energy Markets and Grids*, 2017, pp. 1–26.
- [4] A. Coffman, A. Bušić, and P. Barooah, "Virtual energy storage from TCLs using QoS preserving local randomized control," in 5th ACM International Conference on Systems for Built Environments (BuildSys), November 2018, p. 10.
- [5] J. L. Mathieu, S. Koch, and D. S. Callaway, "State estimation and control of electric loads to manage real-time energy imbalance," *IEEE Transactions on Power Systems*, vol. 28, pp. 430–440, 2013.
- [6] A. Aghajanzadeh and P. Therkelsen, "Agricultural demand response for decarbonizing the electricity grid," *Journal of Cleaner Production*, vol. 220, pp. 827 – 835, 2019.
- [7] Z. E. Lee, Q. Sun, Z. Ma, J. Wang, J. S. MacDonald, and K. Max Zhang, "Providing Grid Services With Heat Pumps: A Review," ASME Journal of Engineering for Sustainable Buildings and Cities, vol. 1, no. 1, 01 2020, 011007.
- [8] H. Hao, A. Kowli, Y. Lin, P. Barooah, and S. Meyn, "Ancillary service for the grid via control of commercial building HVAC systems," in *American Control Conference*, June 2013, pp. 467–472.
- [9] S. Bashash and H. K. Fathy, "Modeling and control of aggregate air conditioning loads for robust renewable power management," *IEEE Transactions on Control Systems Technology*, vol. 21, no. 4, pp. 1318–1327, 2012.
- [10] H. Hao, B. M. Sanandaji, K. Poolla, and T. L. Vincent, "Aggregate flexibility of thermostatically controlled loads," *IEEE Transactions on Power Systems*, vol. 30, no. 1, pp. 189–198, Jan 2015.
- [11] M. Liu, Y. Shi, and X. Liu, "Distributed MPC of aggregated heterogeneous thermostatically controlled loads in smart grid," *IEEE Transactions on Industrial Electronics*, vol. 63, no. 2, pp. 1120–1129, 2016.
- [12] A. Bušić and S. Meyn, "Distributed randomized control for demand dispatch," in *IEEE conference on decision and control*, 2016, pp. 6964– 6971
- [13] E. Benenati, M. Colombino, and E. Dall'Anese, "A tractable formulation for multi-period linearized optimal power flow in presence of thermostatically controlled loads," arXiv preprint arXiv:1908.09167, 2019
- [14] M. S. Nazir and I. Hiskens, "Analysis of synchronization in load ensembles," *Electric Power Systems Research*, vol. 190, p. 106779.
- [15] L. C. Totu, R. Wisniewski, and J. Leth, "Demand response of a TCL population using switching-rate actuation," *IEEE Transactions on Control Systems Technology*, vol. 25, no. 5, pp. 1537–1551, 2017.
- [16] E. C. Kara, M. Bergés, and G. Hug, "Impact of disturbances on modeling of thermostatically controlled loads for demand response," *IEEE Transactions on Smart Grid*, vol. 6, no. 5, pp. 2560–2568, 2015.
- [17] H. K. Versteeg and W. Malalasekera, An introduction to computational fluid dynamics: the finite volume method. Pearson education, 2007.